A&A 391, 675–680 (2002)
DOI: 10.1051/0004-6361:20020691

Astronomy & Astrophysics

H_2 formation and excitation in the diffuse interstellar medium

C. Gry[1,2], F. Boulanger[3], C. Nehmé[3], G. Pineau des Forêts[3], E. Habart[3], and E. Falgarone[4]

[1] ISO Data Center, ESA Research and Scientific Support Department, PO Box 50727, 28080 Madrid, Spain
[2] Laboratoire d'Astrophysique de Marseille, BP 8, 13376 Marseille Cedex 12, France
[3] Institut d'Astrophysique Spatiale, Université Paris Sud, Bat. 121, 91405 Orsay Cedex, France
[4] Ecole Normale Superieure, Laboratoire de Radioastronomie, 24 rue Lhomond, 75231 Paris Cedex 05, France

Received 2 October 2001 / Accepted 6 May 2002

Abstract. We use far-UV absorption spectra obtained with FUSE towards three late B stars to study the formation and excitation of H_2 in the diffuse ISM. The data interpretation relies on a model of the chemical and thermal balance in photon-illuminated gas. The data constrain well the nR product between gas density and H_2 formation rate on dust grains: $nR = 1$ to 2.2×10^{-15} s^{-1}. For each line of sight the mean effective H_2 density n, assumed uniform, is obtained by the best fit of the model to the observed $N(J = 1)/N(J = 0)$ ratio, since the radiation field is known. Combining n with the nR values, we find similar H_2 formation rates for the three stars of about $R = 4 \times 10^{-17}$ cm^3 s^{-1}.
Because the target stars do not interact with the absorbing matter we can show that the H_2 excitation in the $J > 2$ levels cannot be accounted for by the UV pumping of the cold H_2 but implies collisional excitation in regions where the gas is much warmer. The existence of warm H_2 is corroborated by the fact that the star with the largest column density of CH^+ has the largest amount of warm H_2.

Key words. ISM: molecules – ISM: clouds – ISM: lines and bands – ISM: individual objects: chamaeleon – ultraviolet: ISM – stars: individual: HD 102065, HD 108927, HD 96675

1. Introduction

The H_2 formation is a key process for the understanding of the thermal and density structure as well as the chemical evolution of the interstellar medium (ISM). The H_2 formation rate was first estimated through the modelling of the hydrogen recombination on dust surfaces (e.g. Hollenbach et al. 1971). Based on an analysis of Copernicus observations of atomic and molecular hydrogen in the local diffuse clouds, Jura (1975a) proposed an H_2 formation rate ($R = 3{\times}10^{-17}$ cm^3 s^{-1}) which corresponds to the Hollenbach et al. (1971) prediction for a total grain surface of 10^{-21} cm^2/H and a recombination efficiency of 0.5.

The excitation of the H_2 rotational levels from the ground state observed in absorption in the UV is a diagnostic of physical conditions. In diffuse clouds, the low J lines provide a measure of the gas temperature while the excitation of the $J > 2$ levels is generally interpreted as a result of the fluorescence cascade following H_2 pumping by the UV radiation from the target stars. But collisional excitation in shocks driven by the star have also been considered.

Since the pioneering work of Black & Dalgarno (1976) on which the Jura analysis of Copernicus data is based, much progress has been made in the modelling of H_2 in space, in particular about the fluorescence cascade after UV pumping of electronic transitions and collisional deexcitation rates (Combes & Pineau des Forêts 2000). The *Far Ultraviolet Spectroscopic Explorer* (FUSE) is also now providing new UV absorption observations of Galactic H_2 superseding the Copernicus observations by their sensitivity (Snow et al. 2000; Shull et al. 2000; Rachford et al. 2001). The topic of H_2 formation and excitation has also been revived by the observation of the mid-infrared transitions between the rotational levels of the vibrational ground state. These data have been used to estimate the H_2 formation rate in warm photo-dissociation regions at the surface of molecular clouds (Draine & Bertoldi 1999; Habart et al. 2002) where the gas and the dust are both warmer than in the diffuse ISM and thus where the H_2 formation efficiency or the processes involved might differ. ISO observations are not sensitive enough to detect the mid-IR H_2 line emission in the low to moderate column density lines of sight studied in the UV but they have allowed to detect an extended warm H_2 component away from star forming regions across the Galaxy (Verstraete et al. 1999) and in the edge-on galaxy NGC 891 (Valentijn & van der Werf 1999). The Galactic data has been interpreted as evidence for the existence of warm H_2 gas heated by the dissipation of kinetic turbulent energy.

In this paper, we re-consider the question of H_2 formation and excitation in the diffuse ISM by analysing FUSE observations of three late B stars located behind the Chamaeleon clouds. IRAS images show that these stars unlike most earlier type stars usually observed in the UV are truely background field stars that do not interact with the matter responsible for the absorption and that do not contribute to the incident radiation field. These three stars were part of a larger sample of Chamaeleon lines of sight observed with IUE to correlate the UV extinction curve with changes in the dust size distribution

Send offprint requests to: C. Gry,
e-mail: cgry@iso.vilspa.esa.es

Table 1. Interstellar absorption toward the stars. Column densities are in cm^{-2}. CH and CH^+ column densities were derived from high resolution (R = 110 000) optical spectra obtained with the ESO 3.6 m telescope and the Coude Echelle Spectrometer. The C I column densities were derived from HST GHRS observations (Gry et al. 1998). The total column density, N_{total}, has been derived from $E(B-V)$, $N_{total} = 5.8 \times 10^{21}\ E(B-V)$.

	HD 102065	HD 108927	HD 96675
Sp. Type	B9IV	B5V	B7V
d(pc)	170	390	250
$E(B-V)$	0.17 ± 0.04	0.23 ± 0.04	0.31 ± 0.03
A_V	0.67 ± 0.12	0.68 ± 0.10	1.1 ± 0.15
R_V	3.9 ± 0.4	3.0 ± 0.2	3.5 ± 0.2
N(CH)	6.3×10^{12}	1.4×10^{13}	2.2×10^{13}
b(CH)	1.9 km s^{-1}	2.2 km s^{-1}	1.6 km s^{-1}
$N(CH^+)$	$1.2\ 10^{13}$	-	2.8×10^{12}
$b(CH^+)$	3.0 km s^{-1}	-	2.2 km s^{-1}
N(CO)	$(7 \pm 3)\ 10^{13}$	-	$>10^{15}$
N(C I)	$(4 \pm 1)\ 10^{14}$	-	$>1.7 \times 10^{15}$
N_{total}	9.9×10^{20}	1.3×10^{21}	1.8×10^{21}
$N(H_2, J=0)$	$2.0 \pm 0.2 \times 10^{20}$	$2.0 \pm 0.2 \times 10^{20}$	$4.9 \pm 0.9 \times 10^{20}$
$N(H_2, J=1)$	$1.4 \pm 0.1 \times 10^{20}$	$1.2 \pm 0.1 \times 10^{20}$	$2.1 \pm 0.6 \times 10^{20}$
$f = \frac{2N(H_2)}{N_{total}}$	0.69 ± 0.12	0.49 ± 0.09	0.76 ± 0.15

traced by the IRAS mid-IR to far-IR colors (Boulanger et al. 1994). The interstellar medium along these lines of sight was further characterized with high resolution optical and ultraviolet absorption spectra with a spectral resolution of 10^5 obtained at ESO and UV spectra with the Goddard high resolution spectrograph on the Hubble Space Telescope (Gry et al. 1998). Characteristics of these lines of sights and previously observed column densities are given in Table 1.

The FUSE data results (Sect. 2) are analysed by modelling the interaction of the gas with the Solar Neighborhood radiation field. This analysis leads on one hand to an estimate of the H_2 formation rate (Sect. 3) and on the other hand to a discussion of the H_2 excitation (Sect. 4) where we argue that H_2 column densities at $J > 2$ cannot be acounted for by UV pumping.

2. Observations and data analysis

High resolution far UV (905–1187 Å) spectra of HD 102065, HD 108927 and HD 96675 have been obtained in April and May 2000 by FUSE observations of respectively 6.8, 6.5 and 10.2 ks, as part of the PI Team Guaranteed Time. FUSE design, data processing and performance have been described in Moos et al. (2000) and Sahnow et al. (2000). The data have been reprocessed with the calibration pipeline version 1.8.7.

To derive the H_2 column densities, we have used the bands located in the best part of the spectra, namely the Lyman (0,0), (1,0), (2,0), (3,0), (4,0) and (5,0) bands. In effect the UV flux of these stars decreases rapidly with wavelength shortward of Lyβ, due to their relatively late types and their interstellar extinction. The stellar Lyβ absorption is so broad and deep in these spectra that it completely wipes away the interstellar line, prohibiting the determination of HI column densities.

The $J = 0$ and $J = 1$ H_2 lines are heavily saturated and their Lorentzian wings allowed us to derive precise column densities for these two levels independently of the gas velocity distribution. They have been measured through profile fitting with the program "Owens" which allows to fit together (blended) lines from different H_2 levels and other species. All available bands are fitted together meaning that the derived column density gives the best fit on all bands together. This allows to decrease the errors mainly due to the uncertainty on the continuum placement because of overlapping wings of adjacent bands. The error bars on column densities have been estimated empirically as the dispersion of the results of five fits performed with different sets of four H_2 bands each.

The derived H_2 column densities are listed in Table 1. An example of the data and the fits is shown in Fig. 1 for the Lyman (1,0) band in the line of sight towards HD 102065.

For the higher excited levels, the lines are less saturated and fall on the flat part of the curve of growth where the column densities depend heavily on the gas velocity distribution. Thanks to high resolution optical observations of the molecules CH and CH^+, we have derived the b-value of the gas responsible for the CH absorption for the three lines of sight and of the gas responsible for the CH^+ absorption for two of them (Table 1). For HD 102065 we also have a measurement of the C I b-value from new high resolution HST-STIS data: b(C I) = 1.8 ± 0.1 km s^{-1}, close to b(CH). We derive the high-J H_2 column densities via a curve of growth analysis by adopting successively the CH and CH^+ b-values. The results are given in Table 2 and the method is illustrated in Fig. 2 in the case of the line of sight toward HD 102065 for which a significantly different b-values have been measured for CH and CH^+. Figure 2 shows the fit of all measurements for levels $J = 2$ to $J = 5$

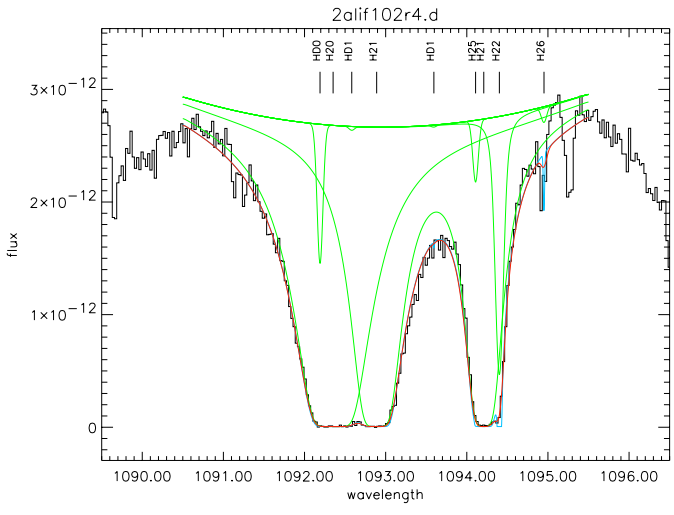

Fig. 1. Example of fit of the H_2 $J = 0$ and $J = 1$ level transitions in the line of sight towards HD 102065. The plot shows the FUSE observations, the synthetic absorption components due to the individual transitions, and the resulting profile. Only one band (Lyman (1,0)) is shown but all available bands are fitted together. Only the column density of the $J = 0$ and $J = 1$ levels (marked H20 and H21) are derived from the fit. The higher H_2 levels (in this case $J = 2$, $J = 5$ and $J = 6$) as well as the HD lines are included in the fit, but their column densities cannot be derived from this fit.

Table 2. H_2 column densities (in cm^{-2}) in the excited ($J \geq 2$) levels, derived from a curve of growth analysis by assuming successively $b = b_{CH}$ and $b = b_{CH^+}$, when available. It is likely that the true $N(H_2)$ is intermediary or close to one of these two estimates.

	HD 102065		HD 108927	HD 96675	
$b_{adopted}$	1.9 km s^{-1}	3.0 km s^{-1}	2.2 km s^{-1}	1.6 km s^{-1}	2.2 km s^{-1}
$N(H_2, J = 2)$	2.6×10^{18}	2.5×10^{18}	1.7×10^{17}	3.3×10^{18}	3.4×10^{18}
$N(H_2, J = 3)$	3.1×10^{17}	1.1×10^{17}	9.3×10^{16}	1.7×10^{17}	8.7×10^{16}
$N(H_2, J = 4)$	5.6×10^{16}	6.0×10^{15}	1.5×10^{15}	4.0×10^{15}	1.4×10^{15}
$N(H_2, J = 5)$	1.2×10^{15}	4.5×10^{14}	$\leq 6 \times 10^{13}$	$\leq 2 \times 10^{14}$	

to the curve of growth corresponding to b(CH) ($b = 1.9$ km^{-1}, top) and $b(CH^+)$ ($b = 3.0$ km^{-1}, bottom). One must keep in mind that significant uncertainties can be attached to these column densities in case the velocity distribution of the excited H_2 gas is different from that of CH and CH^+. However in view of the general good linear correlation of N(CH) with $N(H_2)$ at these column densities (Mattila 1986), and the correlations of $N(CH^+)$ with excited H_2 column densities (see Sect. 4), it is likely that the $J \geq 2$ column densities are intermediary or close to one of these two estimates.

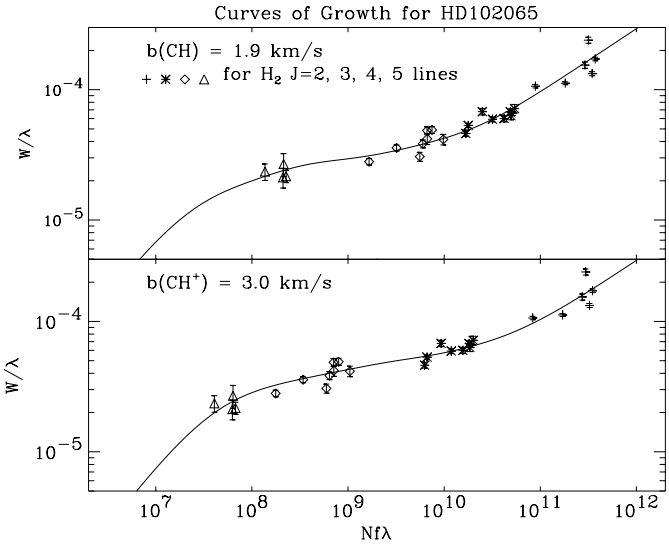

Fig. 2. Curves of growth for the excited levels of H_2. The top plot shows the curve of growth for $b(H_2) = b$(CH) and the bottom plot that for $b(H_2) = b(CH^+)$. The $J > 1$ column densities listed in Table 1 have been derived by fitting the measurements of all $J > 1$ levels together to both curves of growth respectively.

3. H_2 formation

3.1. Determination of the n R product

The local balance between H_2 formation and photo-dissociation can be written as: $n(HI)\, n\, R = n(H_2)\, \beta_0\, G\, S$, where n(HI), $n(H_2)$, n are the atomic, molecular and total hydrogen densities ($n = n(HI) + 2\, n(H_2)$), R the H_2 formation rate, β_0 is the Solar Neighborhood value of the H_2 photo-dissociation rate in the absence of shielding, G is the radiation field value in Solar neighborhood units and S a shielding factor including dust extinction and H_2 self-shielding. For the stars studied here, the IRAS maps show that the stars do not heat the matter responsible for the absorption, we can thus assume that the stars do not contribute to the radiation field and we can take $G = 1$ (Boulanger et al. 1994). For a constant n, integration over the line of sight leads to: $nR = \frac{1}{2}\frac{f}{1-f}\beta_0 \ < S >$ where f is the molecular hydrogen fraction: $f = 2N(H_2)/N_{total}$, where N_{total}, the total column density is derived from the extinction, $N_{total} = 5.8 \times 10^{21}\ E(B-V)$, and $< S >$ is the mean shielding factor. From this formula, one thus sees that the product nR can be derived from the measured molecular hydrogen fraction f.

Practically a model is necessary to determine the abundance and distribution of H_2 molecules over its ro-vibrational levels as a function of depth into the cloud and thereby derive the nR product from f. We have used an updated version of the stationary model developed by Abgrall et al. (1992) and Le Bourlot et al. (1993). The model assumes a semi-infinite plane parallel geometry and solves the equations of thermal and chemical balance iteratively as a function of depth into the cloud. Transfer in the H_2 lines (50 ro-vibrational levels are included in these calculations) and dust extinction are taken into account. The far UV extinction curves used in the models are specific for each star and present a wide variety in terms of 2200 Å bump and far UV rise. These curves are extrapolations of fits to the IUE extinction curves performed by Boulanger et al. (1994). The chemical network includes 100 species and 775 reactions. To take into account UV penetration from two sides, we run models with half the total extinction and multiply all integrated column densities by two. For all calculations, we have assumed a constant gas density through the line of sight. Since we can assume $G = 1$, the model has only two free parameters, the gas density n and the product nR. The gas kinetic temperature is calculated in the model at each depth assuming local equilibrium between heating and cooling processes. The dominant heating process is the photo-electric effect on small grains. Heating by dissipation of turbulent kinetic energy is not included. Model results are shown in Fig. 3 for the line of sight towards HD 108927, where the computed H_2 fraction f is plotted versus the product nR. A comparison of the model results for $n = 20$ and 100 cm^{-3} illustrates the density independence of the relationship. The horizontal lines in the figure represent the measured f with its error bar (from Table 1). The intersections of these lines with the model results define the range for nR. We have used the model to quantify the uncertainties on the product nR related to the line of sight extinction and the far-UV radiation field. We find that the error bar on the A_V measurement translates into an uncertainty of ±50% on nR.

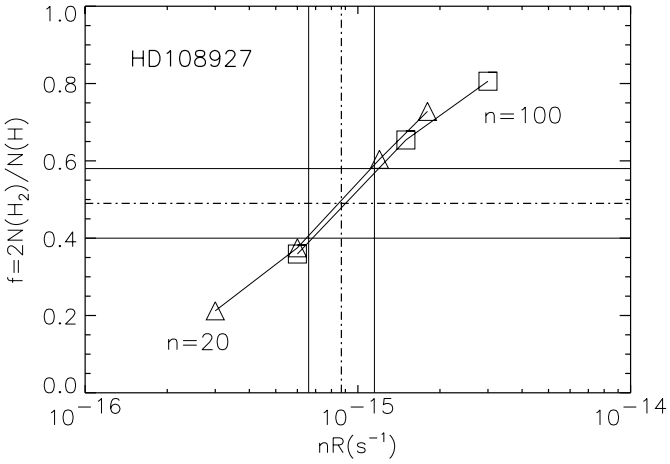

Fig. 3. Determination of the nR product from the H_2 fraction f for HD 108927. The triangles and square symbols represent model calculation for n = 20 and 100 cm^{-3}, respectively.

An uncertainty of a factor 2 on the far-UV radiation field intensity, which is a reasonable assumption, translates into an error-bar of the same amplitude on nR. We thus consider that within the framework of the model, a factor of 2 is the magnitude of the error-bar on nR. Additional systematic errors could be coming from the simplifying assumptions made in the model. These are of course impossible to quantify.

The nR values derived for the three stars are listed in Table 3. Their scatter is of a factor of 2, comparable to the uncertainty on the individual measurements. Jura (1975b) had found a much larger scatter with values from 5×10^{-16} to 3×10^{-14} s^{-1}. The dispersion of Jura's values might be partly due to changes in the G value among the lines of sight towards the very luminous stars observed by Copernicus.

3.2. Determination of R from the H_2 density estimate

To determine the H_2 formation rate R one must complement the nR values with an estimate of the gas density n.

The gas density n is the second free parameter of the model. Density governs the cooling rate and the assumption of thermal balance makes the gas density and temperature uniquely related at each depth once the external radiation field is given. Any tracer of the gas temperature is therefore also a tracer of the density. We thus determine the gas density by fitting the model to the column density ratio of the two first levels, $N(J = 1)/N(J = 0)$, known to be an indicator of temperature. Figure 4 illustrates the best fits, corresponding to the density values indicated in each diagram. Note that in the model the temperature is not uniform, its value is determined at each depth by the thermal balance. The temperature T_B indicated in Fig. 4 is that of the shown Boltzmann distribution corresponding to the $N(J = 1)/N(J = 0)$ ratio value.

The R values derived for the three lines of sight, based on these density estimates are listed in Table 3. This determination of n assumes that the ortho to para H_2 ratio is at its equilibrium value and is therefore very sensitive to the temperature, which is itself, within the assumption of thermal balance, very sensitive to the gas density. Within the model framework, the H_2 $J = 1$ and 0 column density ratio constrains density within about 20%, an uncertainty smaller than that on the product nR. The uncertainty on R is thus governed by the uncertainty on nR: about a factor of 2.

Table 3. H_2 formation rate R from the product nR and the density n estimated from $N(H_2, J = 1)/N(H_2, J = 0)$.

Etoile	HD 102065	HD 108927	HD 96675
nR (s^{-1})	2.3×10^{-15}	0.87×10^{-15}	2.0×10^{-15}
n(cm^{-3})	50	28	50
R(cm^{3}s^{-1})	4.5×10^{-17}	3.1×10^{-17}	4.0×10^{-17}

The values of R for the three lines of sight are close to each other and close to the values found by Jura (1975a) but with significantly lower uncertainties. Note nevertheless that the derivation of R from nR is valid within the hypothesis that the density is homogeneous in the molecular gas. This might not be the case. Indeed, for HD 102065 for which we have been able to derive three other independent density estimates from the comparison of model calculations and measured quantities (namely N(C I), N(CH) and the C I fine structure level population from Gry et al. 1998), there is a scatter of a factor of three among the four density estimates. This scatter might well reflect a density inhomogeneity along the line of sight but could also result from other model shortcomings, in particular in our understanding of the chemistry in diffuse clouds.

The nR values directly translate into an H_2 formation timescale of $1/(nR) \sim 2 \times 10^7$ yrs. For the three stars it is a few times larger than the dynamical timescale ($\sim 10^6 L(\mathrm{pc})/b(\mathrm{km\,s^{-1}})$ yrs) set by turbulent motions on the scales of the absorbing clouds ($L = N/n \sim 10$ pc). The model tells us that the photodissociation timescale is larger than the H_2 formation timescale especially in the shielded layers of the cloud (the dissociation timescale goes from about 3×10^7 yrs to about 3×10^8 yrs for A_V from 0.3 to 1). On the other hand the timescale of ortho to para conversion through proton exchange reactions with protonated ions (e.g. H^+ and H_3^+, Gerlich 1990) is much shorter (0.2 to 2×10^5 yrs). Consequently, the observed H_2 abundance may not correspond to the equilibrium value between formation and destruction and by assuming equilibrium in our interpretation we could be overestimating R and the nR product. Study of a larger sample of stars could reveal scatter in the R and nR values reflecting various states of evolution.

4. Warm H_2 gas

The excitation diagrams of Fig. 4 show that the H_2 column densities derived from the observations for $J > 2$ are all significantly higher than the model values. This is true for our two determinations of H_2 column densities, the highest based on the Doppler parameter of CH and the lowest based on that of CH^+ (see Sect. 2). This means that H_2 excitation by UV pumping and H_2 formation on grains as computed with the model does not account for the $J > 2$ H_2 column densities. With the model, we checked on HD 102065 that to populate these

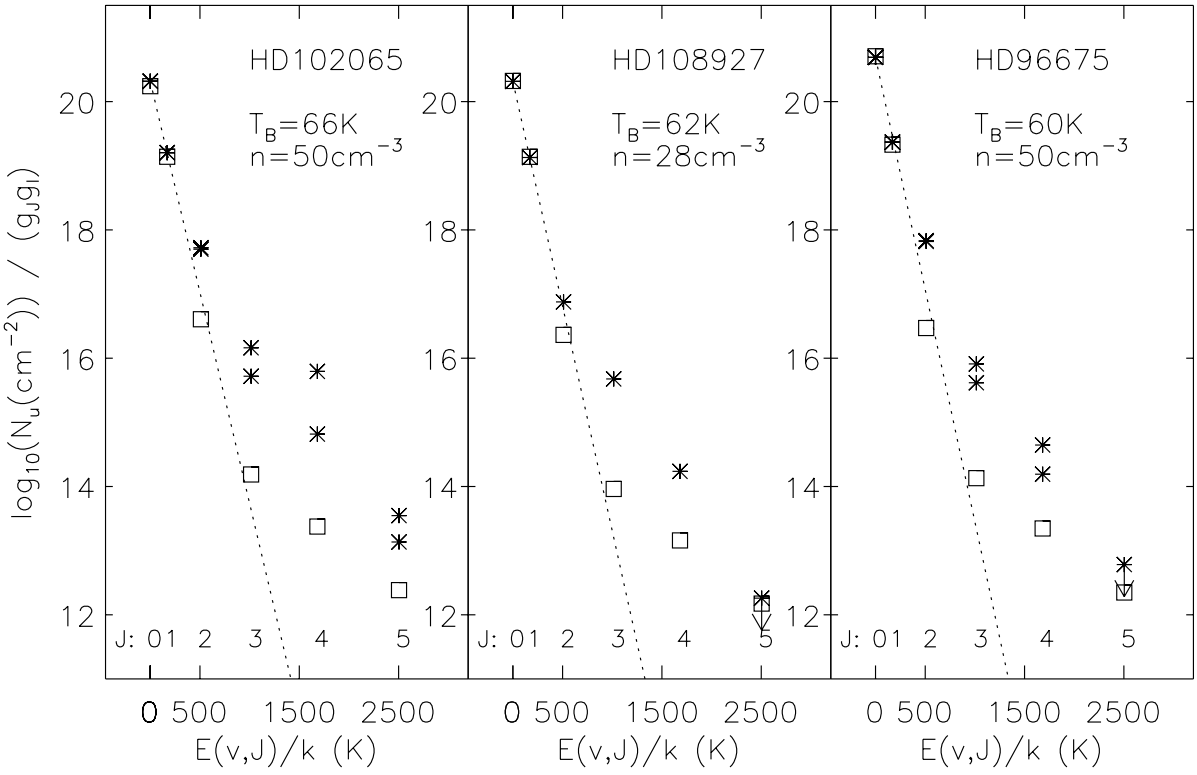

Fig. 4. H_2 excitation diagrams. The asterisks represent the measured column densities listed in Table 1 for $J = 0$ and $J = 1$ and in Table 2 for the higher J levels within the two assumptions $b(H_2)_{ex} = b(CH)$ (higher values) and $b(H_2)_{ex} = b(CH^+)$ (lower values). The squares represent the model that best fits the $J = 0$ and $J = 1$ observations and corresponds to the density indicated. The dashed line is the Boltzmann distribution for the temperature T_B corresponding to the observed $N(J = 1)/N(J = 0)$ ratio.

levels by UV pumping alone (with no collisional deexcitation) we would have to increase the radiation field to a G value of 17 to reproduce the column densities derived with b(CH) and to a G value of 9 to reproduce the column densities derived with $b(CH^+)$. Such values are clearly incompatible with the IRAS dust data because no enhanced IR dust emission is found at the position of the stars and the ratio between the 100 μm cloud brightness and extinction is within the range of values observed over the high Galactic sky. We have checked also that we cannot reproduce the measured $J = 2$ level populations even if all the H_2 binding energy (4.48 eV) is transformed in H_2 internal excitation.

We thus infer the existence of warm gas along the three lines of sight, where the $J > 2$ H_2 levels are populated by collisional excitation. This statement relies on the validity of the H_2 column densities determinations. In the absence of any direct information, one cannot exclude that the H_2 velocity distribution is broader than that of both CH and CH^+ and consequently that even the lowest set of values in Table 2 are larger than the true H_2 column densities. However, we consider unlikely that the H_2 velocity distribution could be such that there is no need for warm H_2 gas because the detection of CH^+ in the direction of both HD 96675 and HD 102065 where it has been looked for is an independent evidence for the existence of a warm H_2 component along these lines of sight. If one considers only collisional excitation, the H_2 excitation temperature is lower than the true gas temperature for densities below the critical densities of each level. The temperature of the warm gas thus needs to be at least equal to the H_2 excitation temperature derived from the $J = 3$ to 5 levels, i.e. between 200 and 240 K for the three stars.

Our conclusion about H_2 excitation at $J > 2$ levels differs from a common interpretation of UV H_2 absorption lines (e.g. Jura 1975b) where it is assumed that the high J levels are mainly populated by pumping through UV photons of the target stars. For our sample of stars we are able to rule out this interpretation, because the FUSE sensitivity allowed us to observe late B stars which do not interact with the absorbing matter, thus lines of sight for which the UV radiation field strength is constrained to be close to the mean Solar Neighborhood value.

The existence of warm H_2 gas within the diffuse ISM has been considered along many lines of sight to account for the observed column densities of CH^+. The observed abundance of CH^+ is a well known problem of interstellar chemistry. The only efficient path for CH^+ formation is the highly endothermic (4640 K) reaction between C^+ and H_2. Further, CH^+ is efficiently destroyed by reaction with H_2 once it is formed. One thus considers that CH^+ only exists in significant abundance where the molecular gas is warm. Away from hot stars, localized volumes of warm gas can be created and sustained by dissipation of the gas kinetic energy. Formation of CH^+ have been quantitatively investigated in the specific cases where dissipation occurs within MHD shocks (e.g. Flower & Pineau des Forêts 1998) or coherent vortices in MHD turbulence (Joulain et al. 1998). In these models the temperature of the warm gas and the ratio between CH^+ and warm H_2 column

Table 4. Abundance of excited H_2 gas. $N(H_2)_{ex}$ (in cm^{-2}) is the sum of the $J = 3$ to 5 column densities from Table 1. The last column (ISO) refers to an infrared observation of a long line of sight through the Galaxy (from Falgarone et al. 2002).

	HD 102065	HD 108927	HD 96675	ISO
$N(H_2)_{ex}$	$1.7 - 3.7 \times 10^{17}$	1.0×10^{17}	$0.9 - 1.7 \times 10^{17}$	7.7×10^{18}
A_V	0.67	0.68	1.1	18
$\frac{N(H_2)_{ex}}{A_V}$	$2.5 - 5.4 \times 10^{17}$	1.5×10^{17}	$0.8 - 1.6 \times 10^{17}$	4.3×10^{17}

densities depends strongly on local physical conditions (e.g. shock velocity, gas density, magnetic field value). The addition of H_2 excitation studies provides a mean to constrain these models and can thus help understand the physics of kinetic energy dissipation in the diffuse ISM.

For each line of sight we have computed and listed in Table 4 a total column density of excited H_2 gas ($N(H_2)_{ex}$) by summing the column densities in the $J = 3$ to 5 levels. The range of values corresponds to the two assumptions used for the determination of H_2 column densities (see Sect. 2). The fact that CH^+ must form in warm H_2 gas makes us consider the lowest value of $N(H_2)_{ex}$, those obtained for the CH^+ Doppler parameter, to be the most realistic estimate. For HD 108927, in the absence of CH^+ observation only the higher estimate is listed. Note that in all cases the excited H_2 gas represents a very small fraction of the total gas. We have not attempted to separate the respective contributions of UV pumping in the cold gas and truly warm gas to the column densities of excited H_2. The excitation diagrams in Fig. 4 show that UV pumping is always a minor contribution.

Based on Copernicus data, Frisch & Jura (1980) suggested a correlation between the column densities of H_2 in the $J = 5$ level and CH^+. They pointed out that CH^+ is particularly abundant in regions with large amounts of rotationally excited H_2. This result has been confirmed by Lambert & Danks (1986) who compared the column densities $N(CH^+)$ and $N(H_2, J)$ for the rotational levels $J = 0 - 5$ in a larger sample of sight-lines. They concluded that the rotationally excited H_2 is a tracer for those hot H_2 molecules that initiate CH^+ formation. Both lines of sight of our study, HD 102065 and HD 96675, for which the CH^+ column density is known, fit within the dispersion of the Lambert & Danks (1986) correlation diagrams. Note that the Lambert & Danks' sample consist of luminous stars for which one cannot exclude that the excited H_2 gas results from the interaction (UV pumping and shock) of the star with its surrounding medium. Further sight-lines such as those considered here, for which this possibility can be excluded, are needed to physically discuss the correlation between CH^+ column densities and warm H_2 in relation with existing models of CH^+ formation.

One Galactic line of sight not crossing any known star forming region has been observed with the mid-IR spectrometer on board of the Infrared Space Observatory (ISO). This observation lead to the detection of three pure rotational lines of the H_2 ground state (Verstraete et al. 1999; Falgarone et al. 2002). The H_2 populations inferred from these detections are compared with our FUSE results in Table 4. The $N(H_2)_{ex}/A_V$ ratio for the long line of sight through the Galaxy is a factor 5 and 2 higher that the lower estimates listed for HD 96675 and HD 102065. We thus find along these two sight-lines a fraction of warm H_2 gas close to the mean Galactic value derived from the ISO observation. The presence of warm H_2 thus seems to be a general characteristics of the diffuse ISM.

Acknowledgements. We are grateful to Martin Lemoine for his profile fitting software Owens and to Vincent Lebrun for reprocessing the data with the FUSE pipeline version 1.8.7. This work is based on data obtained for the Guaranteed Time Team by the NASA-CNES-CSA FUSE mission operated by the Johns Hopkins University.

References

Abgrall, H., Le Bourlot, J., Pineau des Forêts, G., et al. 1992, A&A, 253, 525
Black, J. H., & Dalgarno, A. 1976, ApJ, 203, 132
Boulanger, F., Prévot, M. L., & Gry, C. 1994, A&A, 284, 956
Combes, F., & Pineau des Forêts, G. (eds.) 2000, Molecular Hydrogen in Space (Cambridge University Press)
Draine, B. T., & Bertoldi, F. 1999, in The Universe as seen by ISO, ed. P. Cox, & M. Kessler, ESA-SP 427, 553
Falgarone, E., et al. 2002, in preparation
Flower, D., & Pineau des Forêts, G. 1998, MNRAS, 297, 1182
Frisch, P. C., & Jura, M. 1980, ApJ, 242, 560
Gerlich, D. J. 1990, Chem Phys., 92, 2377
Gry, C., Boulanger, F., Falgarone, E., Pineau des Forêts, G., & Lequeux, J. 1998, A&A, 331, 1070
Habart, E., Boulanger, F., Verstraete, L., & Pineau des Forêts, G. 2002, A&A, in press
Hollenbach, D. J., Werner, M. W., & Salpeter, E. E. 1971, ApJ, 163, 165
Joulain, K., Falgarone, E., Pineau des Forêts, G., & Flower, D. 1998, A&A, 340, 241
Jura, M. 1975a, ApJ, 197, 575
Jura, M. 1975b, ApJ, 197, 581
Lambert, D. L., & Danks, A. C. 1986, ApJ, 303, 401
Le Bourlot, J., Pineau des Forêts, G., Roueff, E., & Flower, D. 1993, A&A, 267, 233
Mattila, K. 1986, A&A, 160, 157.
Moos, H. W., Cash, W. C., Cowie, L. L., et al. 2000, ApJ, 538, L1
Rachford, B. L., Snow, T. P., Tumlinson, J., et al. 2001, ApJ, 555, 839
Sahnow, D. J., Moos, H. W, Ake, T. B., et al. 2000, ApJ, 538, L7
Shull, J. M., Tumlinson, J., Jenkins, E. B., et al. 2000, ApJ, 538, L73
Snow, T. P., Rachford, B. L., Tumlinson, J., et al. 2000, ApJ, 538, L65
Valentijn, E., & van der Werf, P. 1999, ApJ, 522, L29
Verstraete, L., Falgarone, E., Pineau des Forêts, G., et al. 1999, in The Universe as seen by ISO, ESA SP-427, 779